Processing and Properties of Carbon Nanotube/ Poly(methyl methacrylate) Composite Films

Jing Liu,* Asif Rasheed, Marilyn L. Minus, Satish Kumar

School of Polymer, Textile and Fiber Engineering, Georgia Institute of Technology, Atlanta, Georgia 30332-0295

Received 21 January 2008; accepted 23 July 2008
DOI 10.1002/app.29372
Published online 22 December 2008 in Wiley InterScience (www.interscience.wiley.com).

ABSTRACT: A systematic study of the reinforcement of single-walled carbon nanotubes (SWNTs), multiwalled carbon nanotubes, and vapor-grown carbon nanofibers (VGCNFs) in poly(methyl methacrylate) (PMMA) is reported. SWNT/PMMA composite films with various SWNT concentrations (from 0.5 to 50 wt % with respect to the weight of PMMA) were processed from nitromethane. Two types of SWNTs were used: SWNT-A, which contained 35 wt % metal catalyst, and SWNT-B, which contained about 2.4 wt % metal catalyst. Properties of different nanotubes containing composites were compared with 15 wt % carbon nanotubes (CNTs). Property enhancement included electrical conductivity, mechanical properties, and solvent resistance. The thermal degradation of PMMA in the presence of CNTs in air and nitrogen environments was studied. No variation in the thermal degradation behavior of PMMA/CNT was observed in nitrogen. The peak degradation temperature increased for the composites in air at low CNT loadings. Dynamic and thermomechanical properties were also studied. At a 35 wt % SWNT loading, a composite film exhibited good mechanical and electrical properties, good chemical resistance, and a very low coefficient of thermal expansion. Property improvements were rationalized in terms of the nanotube surface area. Composite films were also characterized with Raman spectroscopy. © 2008 Wiley Periodicals, Inc. J Appl Polym Sci 112: 142–156, 2009

Key words: mechanical properties; nanocomposites; thermal properties

INTRODUCTION

Typically, carbon nanotubes (CNTs) exist as single-walled carbon nanotubes (SWNTs),[1,2] double-walled CNTs,[3,4] and multiwalled carbon nanotubes (MWNTs).[5] Another type of important carbon nanofiller is vapor-grown carbon nanofiber (VGCNF), which was developed in the 1980s.[6–8] CNTs have anisotropic electrical,[9] optical,[10] mechanical,[11] and thermal properties.[12] A number of studies have been reported on dispersing CNTs in poly(methyl methacrylate) (PMMA) by solution[13,14] and melt processing[15] and via *in situ* polymerization.[16,17] The reported property improvements in CNT/PMMA composites vary over a very wide range. For instance, in one study, an 8 wt % SWNT loading resulted in a 100% enhancement of the tensile modulus,[15] whereas in another case, only a 2 wt % SWNT loading was needed to achieve a 100% enhancement in the tensile modulus.[18] The addition of less than a 0.1 wt % SWNT loading to PMMA fibers has been shown to increase the low-temperature (−150°C) modulus from 5 to 7 GPa, whereas at temperatures above the glass-transition temperature (T_g), the modulus essentially remained unchanged. The author attributed these changes to PMMA/SWNT cohesive interactions at low temperatures and not to any morphological changes in PMMA.[18] Drawn PMMA fibers containing a 1 wt % SWNT loading exhibited a dramatic increase in the strain at failure (700%) in comparison with neat PMMA fibers of a similar draw ratio.[19] Functionalized SWNTs have also been used to reinforce PMMA matrix.[20] SWNTs doped with $SOCl_2$ have been used as a reinforcement component.[21] In a pristine SWNT/PMMA composite, a percolation threshold as low as 0.17 wt % was found, with the conductivity value reaching 1700 S/m. When SWNTs were doped with $SOCl_2$, the percolation threshold did not change, but the saturation conductivity reached about 10,000 S/m, and the toughness increased to 6 GJ/m^3, which is 30 times the toughness of pure PMMA. PMMA composites with MWNTs as well as VGCNFs have also attracted significant attention.[16,17,22–27] In this article, a systematic structural, processing, and property study of the reinforcement of SWNTs, MWNTs, and VGCNFs in PMMA is reported.

EXPERIMENTAL

Two types of SWNTs, obtained from Unidym, Inc. (Menlo Park, CA), were used without further

*Present address: Department of Chemistry, University of Wisconsin, 800 West Main Street, Whitewater, WI 53190

Correspondence to: S. Kumar (satish.kumar@ptfe.gatech.edu).

Contract grant sponsor: Air Force Office of Scientific Research.

TABLE I
Recipe and Preparation Conditions for the PMMA, SWNT-A/PMMA, and SWNT-B/PMMA Composite Films

SWNT-A/ SWNT-B (wt %)	SWNT-A/ SWNT-B (mg)	PMMA (mg)	Nitromethane (mL)	Sonication time (h)	Stirring time (h)
0	0	300	15	0	4
0.5	1.5	300	15	24	4
1	3	297	15	24	4
5	15	285	20	48	4
10[a]	30	270	40	48	4
15[a]	45	255	60	48	4
20	75	225	100	48	4
35	105	195	140	48	4
50	150	150	200	48	4

[a] Concentration at which the SWNT-A/PMMA composite samples were also prepared.

purification (SWNT-A, lot R0231 with 35 wt % metal catalyst, and SWNT-B, lot XO021UA with 2.4 wt % metal catalyst). MWNTs were obtained from Iljin Nanotech Co. (Seoul, Korea), and VGCNFs (PR-24-HT) were obtained from Applied Sciences, Inc. (Cedarville, OH). Thermogravimetric analysis (TGA) of these CNTs in air at a heating rate of 10°C/min showed the decomposition temperatures of SWNT-A, SWNT-B, MWNTs, and VGCNFs to be 422, 570, 626, and 738°C, respectively. PMMA (molecular weight in the range of 95,000 to 150,000 g/mole) was obtained from Cyro Industries (Parsippany, NJ) and also used as received. Nitromethane and toluene were obtained from Sigma–Aldrich Co. (St. Louis, MO) and also used as received.

CNTs were dispersed in nitromethane by sonication (Branson 3510 sonicator, Branson Ultrasonic Corp., Danbury, CT) for a certain amount of time (typically 24–48 h) until an optically homogeneous solution was achieved. To this uniform SWNT/nitromethane dispersion, a PMMA/nitromethane solution was added and mixed by stirring. The optically homogeneous PMMA/SWNT/nitromethane solution was cast onto a glass substrate to form 20–25-μm-thick films. A control PMMA film was also prepared with the same procedure. The resulting films were dried *in vacuo* at 80°C for 2 days. Table I summarizes the experimental conditions for preparing PMMA, SWNT-A/PMMA, and SWNT-B/PMMA films with different SWNT loadings. Similar processing conditions were used for MWNT and VGCNF composites.

For scanning electron microscopy (SEM), films were cut with a blade. Images were obtained on gold-coated cross sections of the films with a Leo 1530 scanning electron microscope (LEO, Oberkochen, Germany). Transmission electron microscopy (TEM) was conducted with a Hitachi HF-2000 (Tokyo, Japan) (operated at 200 kV). For TEM specimen preparation, the SWNT powders were sonicated in ethanol for 10 min, and then a droplet of the dispersion was placed on the lacey carbon-coated copper grids with a loop. The SWNT-B/PMMA composite film (3.53 mg) was soaked in toluene (4 mL) for 5 days to completely disintegrate the film, and then additional toluene (20 mL) was used to dilute a drop of the suspension. A droplet of the diluted suspension was collected on a TEM grid with a loop. An RSA III (Rheometrics Scientific, Piscataway, NJ) was used to measure the tensile properties and the dynamic mechanical properties. The gauge length, film width, and strain rate for the tensile tests were 15 mm, 5 mm, and 10%/min, respectively. Dynamic mechanical analysis was conducted at 0.1, 1.0, and 10.0 Hz with a temperature increment of 2°C/min. The T_g values of the films were measured by both differential scanning calorimetry (DSC; DSC100, TA Instruments) and dynamic mechanical analysis. The coefficient of thermal expansion (CTE) was determined with thermomechanical analysis (TMA Q400, TA Instruments, New Castle, DE) at a stress of 0.35 MPa on 8-mm-long and 2-mm-wide films at a heating rate of 5°C/min. TGA (TGA 2950, TA Instruments) of various films was conducted in air (or in nitrogen) at a heating rate of 10°C/min. In-plane direct-current (dc) electrical conductivity was measured by the four-probe method. The Raman spectra were collected on a Holoprobe Research Raman microscope made by Kaiser Optical Systems, Inc. (Ann Arbor, MI), using a 785-nm excitation wavelength (the laser energy (E_{laser}) = 1.58 eV).

RESULTS AND DISCUSSION

A previous dispersion study using different solvents[28] has shown that a uniform CNT dispersion can be obtained in nitromethane. Optical micrographs of SWNT-B/nitromethane and SWNT-B/

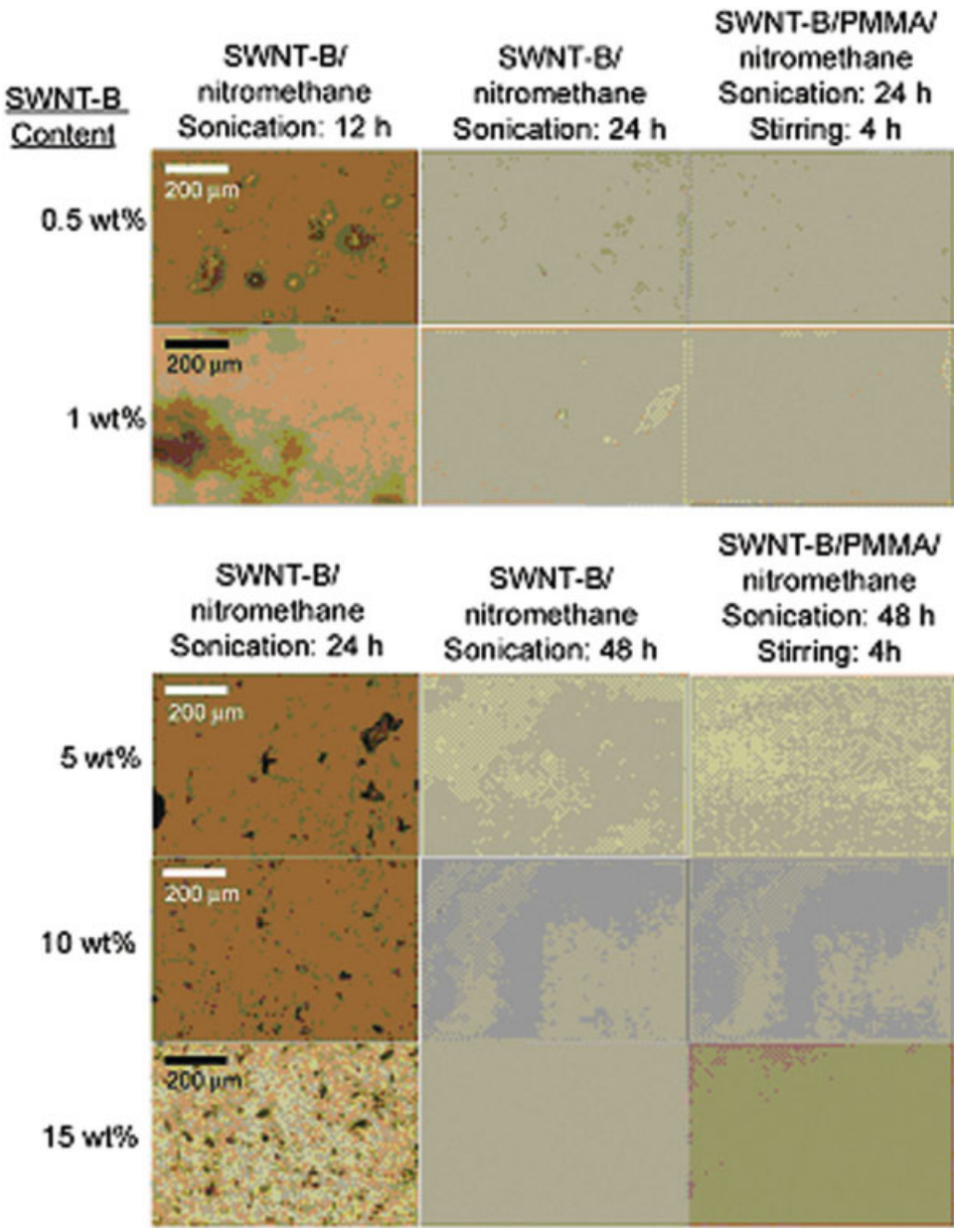

Figure 1 Optical micrographs of SWNT-B/nitromethane and SWNT-B/PMMA/nitromethane dispersions. [Color figure can be viewed in the online issue, which is available at www.interscience.wiley.com.]

PMMA/nitromethane showed homogeneous nanotube dispersions at the micrometer scale (Fig. 1). For samples containing 0.5 or 1.0 wt % SWNT, the sonication time was 24 h. However, for composite samples containing higher nanotube loadings, a 24-h sonication time was not sufficient to achieve a homogeneous dispersion, and so in these cases, 48 h of sonication was used. The ratio of SWNT-B to nitromethane and the sonication time were kept the same for the composites with SWNT-B loadings higher than 1.0 wt %. Similarly, uniform dispersions of other nanotubes were also obtained with a sonication time of 48 h (micrographs not shown). SWNT-B/PMMA films were prepared with a layer-by-layer method. First, 50 mL of an SWNT-B/PMMA/nitromethane solution was cast onto the glass substrate, and the solvent was allowed to evaporate at room temperature (25°C). After 12 h, another 50-mL solution was cast onto this film and allowed to dry, and this eventually resulted in the final film. For example, samples with 20, 35, or 50 wt % nanotubes have two, three, or four layers, respectively.

A high-resolution TEM image of as-received SWNT-A powder is given in Figure 2. The typical size of the metal catalyst in SWNT-A was about 4 nm. SEM images of cross sections of PMMA/SWNT-A composite films (Fig. 3) show uniform nanotube dispersions in the PMMA matrix. According to the

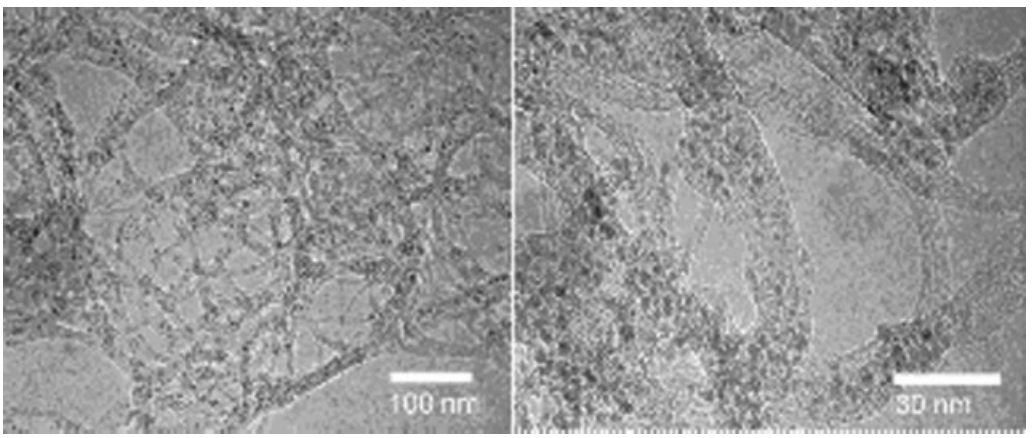

Figure 2 TEM images of SWNT-A powder (low and high magnifications).

mechanical properties for SWNT-A/PMMA composites listed in Table II, the elongation to break of SWNT-A/PMMA composite films was lower than that of the control PMMA film. This is consistent with studies on CNT composite films with polyacrylonitrile (polyacrylonitrile (PAN))[29] and PVA.[29,30] For the composite with a 10 wt % nanotube concentration, the tensile modulus was almost 3 times that of the pure PMMA.

The storage modulus (E') and tan δ curves for PMMA and SWNT-A/PMMA composite films are given in Figure 4. Based on the tan δ peak position, T_g of the composite films with a 10 or 15 wt % nanotube loading was 129°C, whereas that of the control

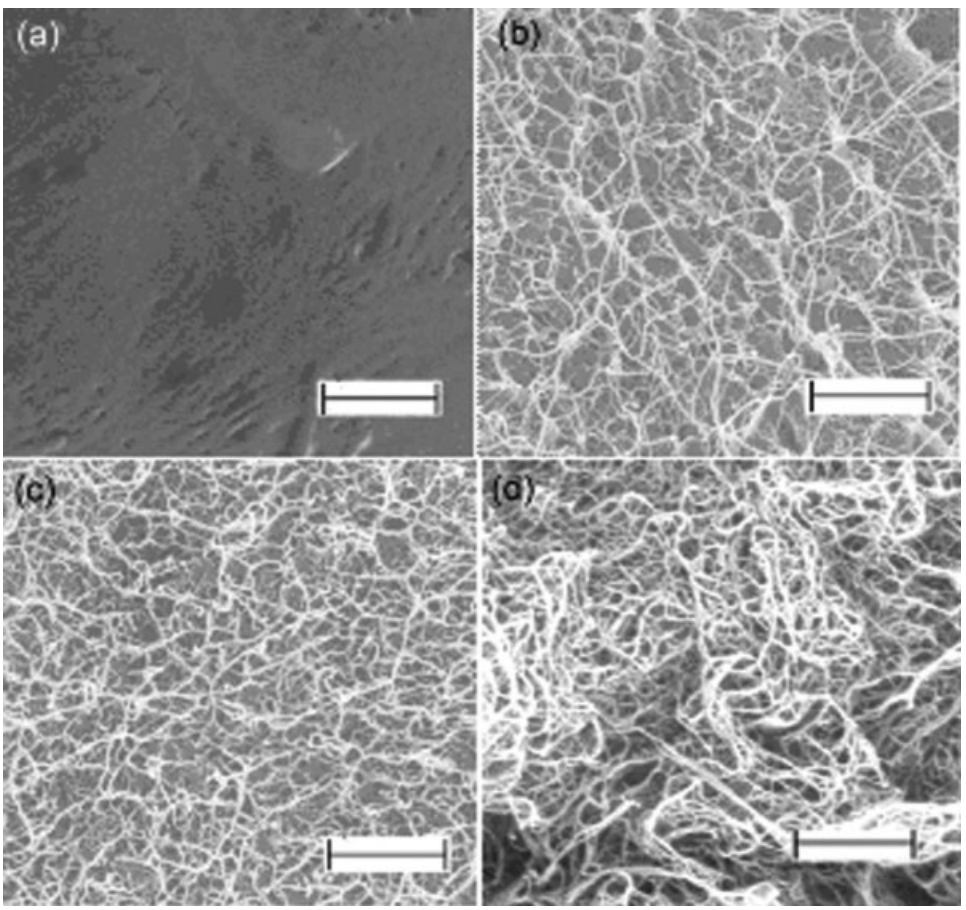

Figure 3 SEM images of cross sections of (a–c) SWNT-A/PMMA composite films at SWNT-A loadings of 0, 10, and 15 wt %, respectively, and (d) SWNT-A powder (scale bar = 1 μm).

TABLE II
Tensile Properties and Densities of the PMMA, SWNT-A/PMMA, and SWNT-B/PMMA Composites

SWNT-B (wt %)	Tensile modulus (GPa)	Tensile strength (MPa)	Elongation at break (%)	Density measured (g/cm^3)
0	1.8 ± 0.1	50 ± 8	3.5 ± 0.5	1.01
1	2.3 ± 0.2	53 ± 9	2.8 ± 0.3	1.03
5	3.4 ± 0.2	56 ± 10	2.5 ± 0.4	1.02
10	4.4 ± 0.2	63 ± 8	2.5 ± 0.7	1.06
	5.1 ± 0.3[a]	51 ± 11[a]	0.9 ± 0.2[a]	1.05[a]
15	5.3 ± 0.2	71 ± 1	2.4 ± 0.2	1.03
	4.1 ± 0.2[b]	23 ± 12[b]	0.6 ± 0.3[b]	1.07[b]
20	5.8 ± 0.2	80 ± 9	2.1 ± 0.5	1.03
35	6.7 ± 0.5	105 ± 8	2.5 ± 0.2	1.01
50	5.7 ± 0.1	86 ± 8	1.8 ± 0.1	1.01

[a] SWNT-A/PMMA (10 wt %) composite film. At a 10 wt % filler loading, the SWNT content was 6.5 wt %, and the rest (3.5 wt %) was iron catalyst.
[b] SWNT-A/PMMA (15 wt %) composite film. At a 15 wt % filler loading, the SWNT content was 9.7 wt %, and the rest (5.3 wt %) was iron catalyst.

PMMA film was 121°C. Tan δ peaks of the composite films also became broader and their magnitudes decreased in comparison with the pure PMMA film. The magnitude of the tan δ peak for the PMMA film, SWNT-A/PMMA (10 wt %) film, and SWNT-A/PMMA (15 wt %) film was 1.78, 0.58, and 0.42, respectively. The decrease in the tan δ magnitude for the composite films suggests suppression of PMMA molecular motion in the presence of CNTs.[31–33] For 10 and 15 wt % SWNT-A/PMMA composite films, the electrical conductivity values were 920 and 1430 S/m, respectively (Table III).

SEM images of cross sections of SWNT-B/PMMA composite films at various SWNT loadings are given in Figure 5(a–h). An SEM image of as-received SWNT-B powder is also given in Figure 5(i). High-resolution TEM images of as-received SWNT-B powder are given in Figure 6(a,b), and an SWNT-B/PMMA (5 wt %) composite film dissolved in toluene is shown in Figure 6(c,d). From these TEM images, we can see that there is no clear evidence of PMMA wrapping or covering SWNT-B bundles. In the literature, several different polymer coatings on SWNTs have been reported. These include PAN,[34] polycarbonate,[35] and polystyrene.[19] The polymer coating behavior suggests good interaction between the polymer and SWNTs. This may suggest that the PMMA–SWNT interaction is weaker than the SWNT interaction with PAN, polystyrene, or polycarbonate. However, further work is needed to confirm this.

For both SWNT-A/PMMA and SWNT-B/PMMA composites, Figures 3, 5, and 6 show that the SWNT structures were still intact even after sonication. However, HR-TEM images in Figure 6 show the effect of nanotube cutting/shortening by sonication. Figure 6(a,b) shows SWNTs before sonication, with

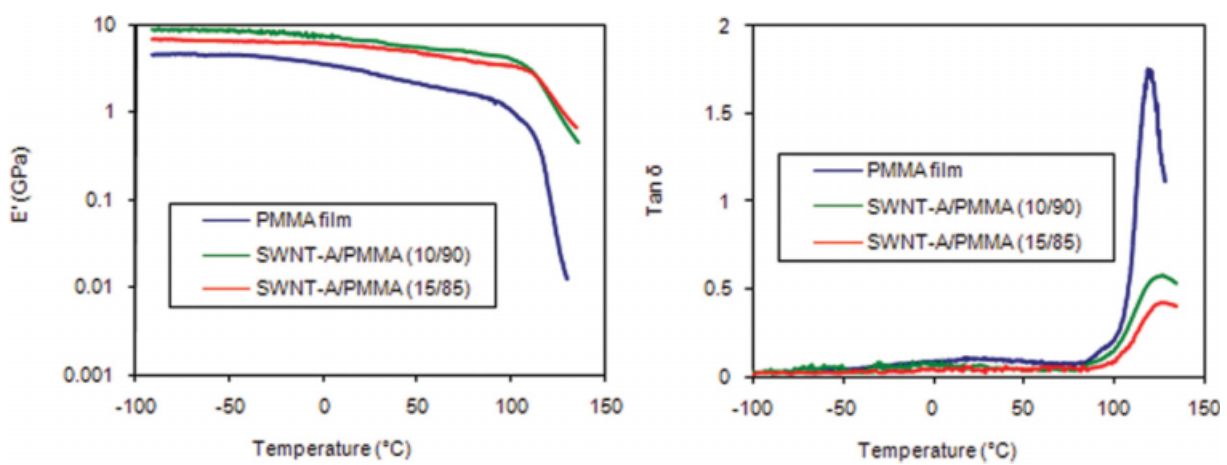

Figure 4 E' and tan δ behavior of PMMA and SWNT-A/PMMA composite films as a function of temperature: (a) a PMMA film, (b) SWNT-A/PMMA (10/90), and (c) SWNT-A/PMMA (15/85). [Color figure can be viewed in the online issue, which is available at www.interscience.wiley.com.]

TABLE III
Electrical Conductivity Values of the SWNT-B/PMMA Composite Films at Different SWNT-B Concentrations

SWNT-B (wt %)	Electrical conductivity (S/m)
0	1.0×10^{-14} [62]
0.5	7.9×10^{-5}
1	7
5	126
10	456 (920)[a]
15	854 (1430)[a]
20	1435
35	3574
50	5783

[a] The electrical conductivities of the SWNT-A/PMMA composites are given in parentheses for comparison.

no ends visible, whereas after sonication, SWNT ends could be observed [Fig. 6(c,d)]. Previous work on PAN/SWNT composite fibers has also shown by both SEM and TEM studies that nanotube structures remain intact even after long sonication times,[34,36] although their length decreases.

The electrical conductivity values of SWNT-B/PMMA composite films with different nanotube loadings are given in Table III. Because the densities of PMMA and SWNTs were comparable, the volume fraction of SWNT-B was taken to be the same as its weight fraction. The inset of Figure 7 is a plot of the conductivity as a function of the SWNT-B volume fraction (V), from which a percolation volume (V_c) of 0.5% was obtained. A plot of the electrical conductivity as a function of $V - V_c$ (Fig. 7) gave an exponent of 1.73, which suggested three-dimensional percolation behavior.

SWNT-A/PMMA films exhibited higher electrical conductivity than SWNT-B/PMMA composites. Because of the higher metal catalyst content in SWNT-A versus SWNT-B, at the same as-received SWNT powder loadings in the PMMA composite films, the SWNT-A samples contained a lower amount of nanotubes than SWNT-B. The metal catalyst in SWNT-A/PMMA also contributed to the electrical conductivity. Literature reports show that carbon-coated iron carbide nanoparticles (typical metal catalysts for SWNT samples) that are approximately 100 nm in size and are embedded in poly(vinyl chloride) have a percolation value of 2.2 wt %.[37] The size of the metal catalyst in SWNT-A was about

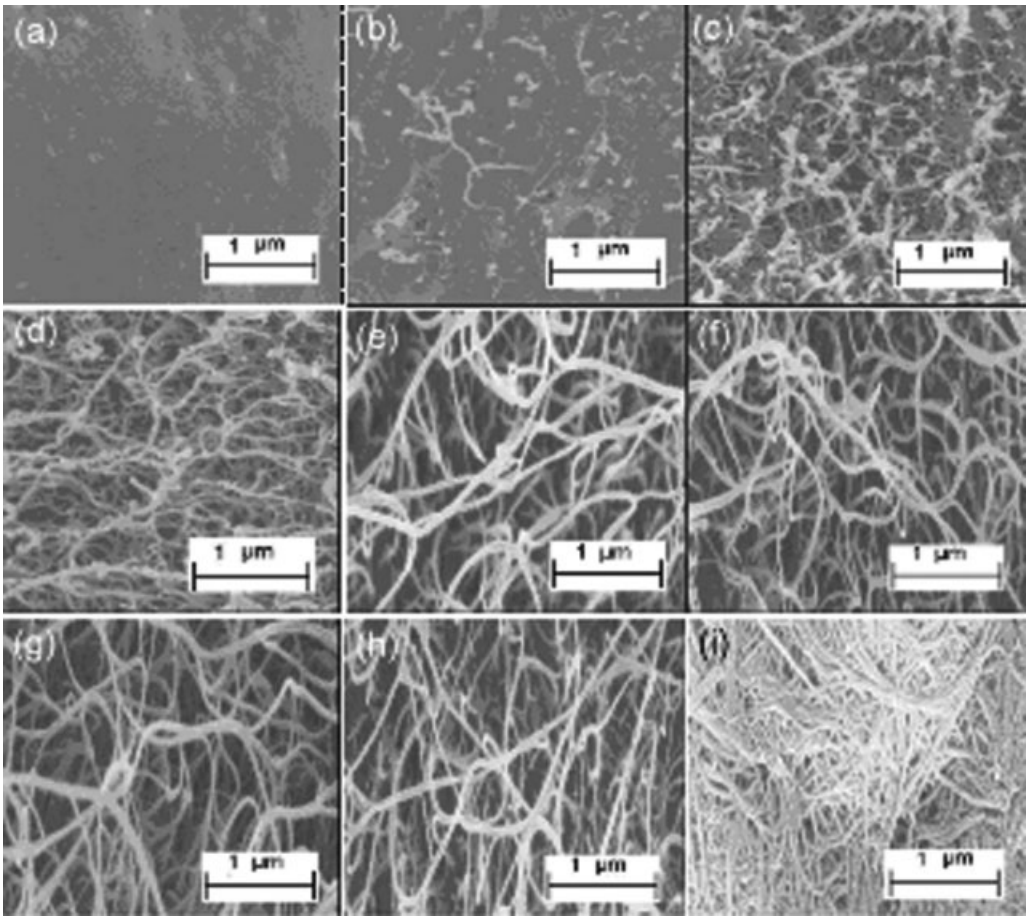

Figure 5 SEM images of cross sections of (a–h) SWNT-B/PMMA composite films at SWNT-B concentrations of 0.5, 1.0, 5.0, 10.0, 15.0, 20.0, 35.0, and 50.0 wt %, respectively, and (i) SWNT-B powder.

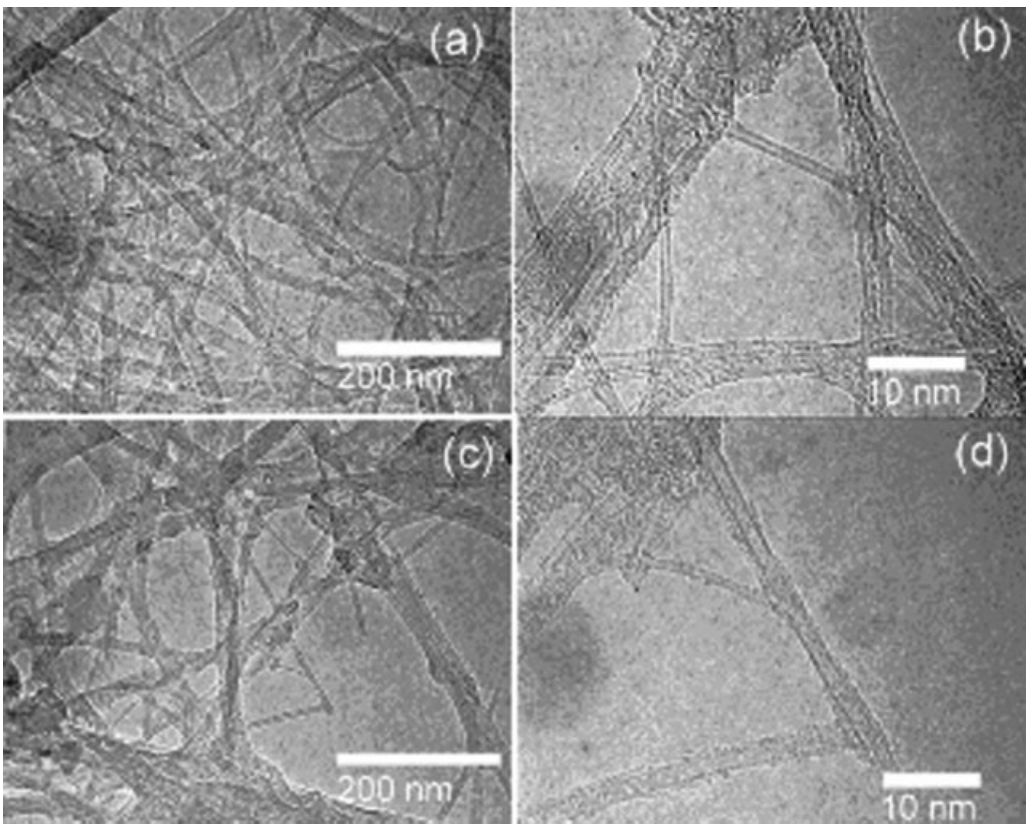

Figure 6 TEM images of (a,b) SWNT-B powder and (c,d) an SWNT-B/PMMA (5 wt % SWNT-B loading) composite film.

4 nm, as determined from a TEM image (Fig. 2). For SWNT-A/PMMA (10/90), the catalyst concentration in the composite was about 3.5 wt % in PMMA, whereas for the 15 wt % SWNT-A/PMMA sample, the catalyst concentration in the composite was 5.3 wt %. According to the previously cited iron carbide study, the amount of metal catalyst in both the 10 and 15 wt % SWNT-A/PMMA composites (3.5 and 5.3 wt %, respectively) was already above the percolation value. These two electrically conductive networks (SWNT-A and metal catalyst) interplayed with each other in PMMA, and this resulted in higher electrical conductivity than that of SWNT-B/PMMA with the same total filler loading. Because the 15% SWNT-A filler contained only 9.7 wt % nanotubes (and 5.3 wt % catalyst), the higher electrical conductivity of this sample (1430 S/m) can even be compared to that of samples containing 10 wt % SWNT-B (456 S/m). This further confirms the electrical conductivity contribution from the catalyst.

The tensile properties of PMMA and SWNT-B/PMMA composites as well as their density values are given in Table II. The elongation at break decreased with the addition of SWNT-B. However, the elongation at break was significantly higher for SWNT-B/PMMA versus SWNT-A/PMMA. We conclude that the presence of the metal catalyst in SWNT-A was the main reason for the lower elongation at break in the PMMA/SWNT-A composites. The tensile modulus and tensile strength of the composite films were higher than those of the control PMMA film. With a 35 wt % SWNT-B loading, the tensile modulus and tensile strength of the composite reached a maximum. Under the current processing scheme, this is the optimum nanotube loading

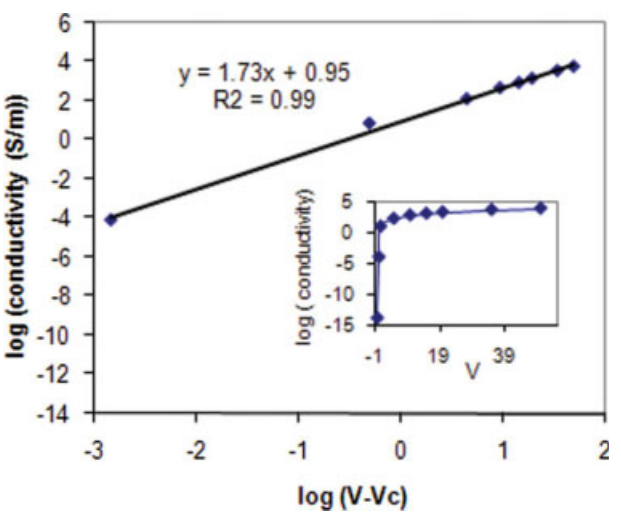

Figure 7 Electrical conductivity of SWNT-B/PMMA composites. [Color figure can be viewed in the online issue, which is available at www.interscience.wiley.com.]

TABLE IV
Tan δ Peak Temperature (*P*) and Tan δ Peak Magnitude (*M*) Values for the PMMA and SWNT-B/PMMA Films at Different Frequencies and Calculated Activation Energies

	0.1 Hz		1 Hz		10 Hz		
SWNT-B (wt %)	*P* (°C)	*M*	*P* (°C)	*M*	*P* (°C)	*M*	Activation energy (kJ/mol)
0	113	1.99	121	1.74	124	1.00	497
5	114	0.85	122	0.72	124	0.48	523
10	115	0.43	123	0.40	128	0.33	449
15	123	0.43	130	0.35	137	0.32	444
20	124	0.35	129	0.29	138	0.28	436
35	128	0.21	133	0.20	137	0.19	501
50	128	0.20	132	0.15	140	0.15	479

for reinforcing PMMA. The properties of a 35% CNT containing PMMA film could be favorable in comparison with the properties of a 60/40 PAN/SWNT film (tensile modulus = 10.9 GPa, tensile strength = 103 MPa, elongation to break = 1.6%, CTE = 1.7 ppm/°C, in-plane dc electrical conductivity = 1.5×10^4 S/m)[29] and those of 100% CNT films processed from sulfuric acid (tensile modulus = 8 GPa, tensile strength = 30 MPa, elongation to break = 0.5%, in-plane dc electrical conductivity = 1×10^5 S/m)[38] and processed from nitric acid (tensile modulus = 5 GPa, tensile strength = 74 GPa, elongation to break = 3%, in-plane dc electrical conductivity = 1.2×10^4 S/m).[39] We also note that the tensile modulus of the CNT films is consistent with theoretical predictions.[40]

Tan δ of the PMMA and composite films as a function of temperature is given in Table IV. For a given SWMT-B/PMMA composite, the tan δ peak position shifted to a higher temperature upon the test frequency increasing, and its magnitude decreased. At a given frequency, the tan δ peak position shifted to a higher temperature and its magnitude decreased with increasing SWNT-B loading. The decrease in the tan δ magnitude suggests the suppression of PMMA molecular motion above T_g.[31–33] T_g activation energies calculated from tan δ versus temperature plots at three frequencies with an Arrhenius equation [$f = A \exp(-\Delta H/RT)$, where f is the frequency, A is a constant, ΔH is the activation energy, T is the temperature, and R is the gas constant] for various samples are listed in Table IV. The activation energies of the SWNT-B/PMMA composites were comparable to that of the PMMA film.

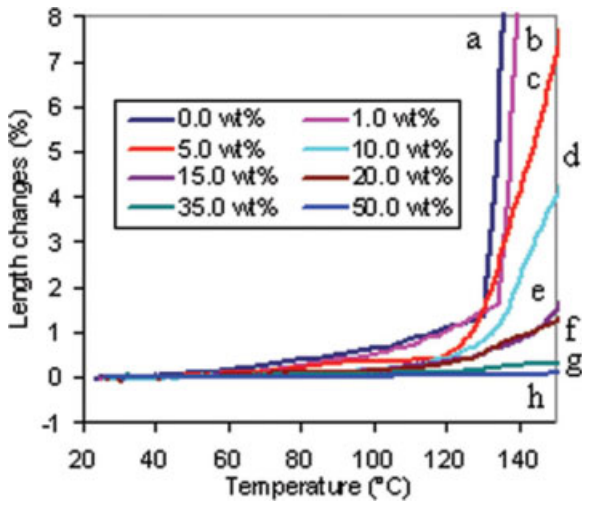

Figure 8 Thermal expansion of PMMA and SWNT-B/PMMA films as a function of temperature under 0.35-MPa stress. The SWNT-B concentration were as follows: (a) 0, (b) 1, (c) 5, (d) 10, (e) 15, (f) 20, (g) 35, and (h) 50 wt %. [Color figure can be viewed in the online issue, which is available at www.interscience.wiley.com.]

Dimensional stability data determined with thermomechanical analysis at a stress of 0.35 MPa and a heating rate of 5°C/min are plotted in Figure 8. The CTEs of PMMA and SWNT-B/PMMA composites at 30 and 105°C are listed in Table V. The composite films exhibited smaller CTEs than pure PMMA. A PMMA film containing 50% CNTs exhibited a room-temperature CTE of 2 ppm/°C, whereas at the same temperature, the in-plane CTE of a 100% PMMA film was 50 ppm/°C. For a 1% length change under 0.35-MPa stress, the temperature increased from 116°C for pure PMMA to 211°C for SWNT-B/PMMA with a 50 wt % SWNT-B loading. T_g values of PMMA and composite films obtained from DSC are given in Table VI. In both heating and cooling

TABLE V
CTEs and Temperatures at a 1% Length Change for PMMA and the SWNT-B/PMMA Composite Films

	CTE (10^{-6}/°C)		
SWNT-B (wt %)	At 30°C	At 105°C	Temperature at a 1% length change (°C)
0	50	152	116
1	32	137	119
5	18	50	127
10	11	80	133
15	9	47	144
20	8	42	144
35	3	24	183
50	2	10	211

TABLE VI
T_g Values of PMMA and the SWNT-B/PMMA Films Determined by DSC

	T_g (°C)	
SWNT-B (wt %)	Second heating cycle	First cooling cycle
0	114.6	107.5
1	114.2	108.8
5	116.7	109.8
10	116.9	111.6
15	119.9	112.1
20	119.6	112.2
35	121.6	114.9
50	121.9	115.0

cycles, a composite film containing 50% CNTs exhibited a T_g that was about 6 to 7°C higher than that for the pure PMMA film. As expected, the tan δ peak temperature values corresponding to the PMMA glass transition (Table IV) were higher than those obtained from DSC. Based on the dynamic mechanical data, T_g of a 50% CNT containing composite film was about 15°C higher than that of the control PMMA film (Table IV). This was comparable to the behavior of a PAN/SWNT (60/40) film, for which an increase of about 15°C was obtained according to the dynamic mechanical data.[29] By comparison, we note that a PAN/SWNT fiber containing 10 wt % SWNTs exhibited a T_g that was 40°C higher than that of the control PAN fiber.[33] The decrease in the tan δ peak magnitude with increasing CNT concentration was similar to behavior reported for PAN[29] and PVA.[41]

The degradation temperatures (T_d's) of SWNT-B, PMMA, and SWNT-B/PMMA composites were determined by TGA (Figs. 9 and 10), and the peak T_d's (in air and nitrogen) are listed in Table VII. T_d for each film was obtained from temperature versus weight derivative curves (not shown). The peak T_d of pure SWNT-B in air was ~ 570°C. In a typical PMMA/SWNT-B TGA curve (not shown), degradation occurs at two different temperatures, one corresponding to the degradation of PMMA and the second corresponding to the degradation of SWNT. T_d of SWNT-B in air varied in the PMMA/SWNT-B composites. With an increase in the SWNT-B loading in the composite, T_d approached that of neat SWNT-B. The last column in Table VII lists the T_d values of SWNT-B in each composite. The peak T_d value of the neat PMMA film in nitrogen was ~ 388°C. Upon the addition of CNTs to the PMMA matrix, a small variation in the peak T_d was observed (382–386°C for composites containing 1, 5, 15, 20, or 50 wt % SWNT-B and 376 and 392°C for composites containing 10 or 35% SWNT-B, respectively), with no particular trend. Costache et al.[42] studied the thermal

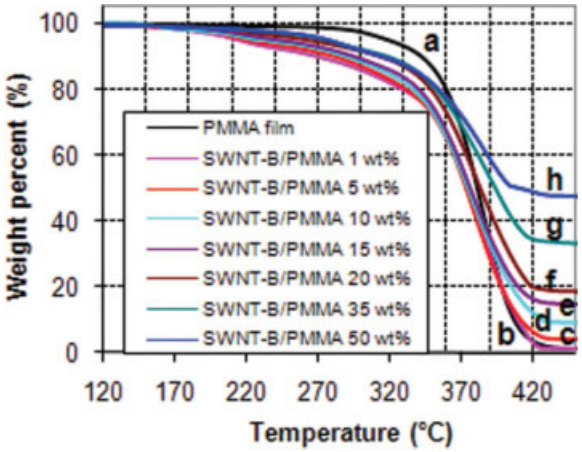

Figure 9 TGA in nitrogen at a heating rate of 10°C/min for SWNT-B/PMMA composites. The SWNT-B concentrations were as follows: (a) 0, (b) 1, (c) 5, (d) 10, (e) 15, (f) 20, (g) 35, and (h) 50 wt %. [Color figure can be viewed in the online issue, which is available at www.interscience.wiley.com.]

degradation mechanism of PMMA in the presence of various nanofillers (clay and CNTs) under a nitrogen atmosphere. The results indicated that the degradation mechanism was not altered in the presence of a nanofiller.

The peak T_d of the neat PMMA film in air was ~ 337°C. The addition of small amounts of CNTs to the PMMA matrix shifted the T_d peak of the resulting composites. For composites containing 1 or 5 wt % SWNT-B, the peak T_d was ~ 370°C (an enhancement of ca. 33°C with respect to neat PMMA). However, increasing the amount of SWNT-B resulted in a decreased peak T_d value of PMMA in the resulting composite (to 357, 355, or 350°C for composites

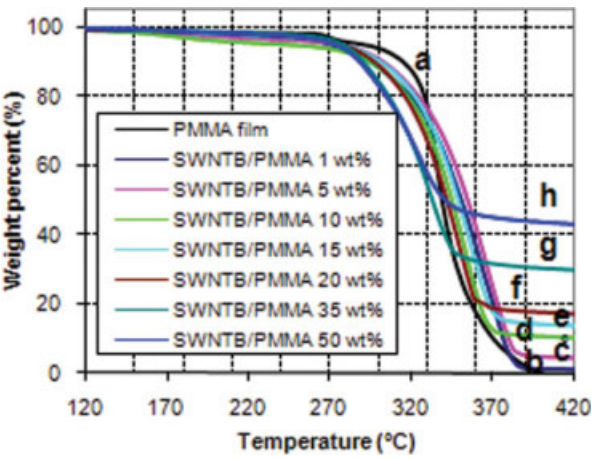

Figure 10 TGA in air at a heating rate of 10°C/min for SWNT-B/PMMA composites. The SWNT-B concentrations were as follows: (a) 0, (b) 1, (c) 5, (d) 10, (e) 15, (f) 20, (g) 35, and (h) 50 wt %. [Color figure can be viewed in the online issue, which is available at www.interscience.wiley.com.]

TABLE VII
T_d Values of Each Component in the SWNT-B/PMMA Composites and Residues at 800°C Determined by TGA in Air and Nitrogen Environments at a Heating Rate of 10°C/min

	T_d of PMMA (°C)				
	In air		In nitrogen		T_d of SWNT-B in PMMA/SWNT-B in air (°C)
SWNT-B (wt %)	T_d	Residue (%)	T_d	Residue (%)	
0	337	0.1	388	0.1	—
1	370	0.4	386	1.0	501
5	370	0.3	382	4.1	508
10	357	0.5	376	9.0	509
15	357	0.4	385	14.1	525
20	350	0.6	383	18.2	529
35	333[a]	1.1	392	32.5	538
50	326[a]	1.2	386	46.7	559
100		2.6		—	570

[a] There was also a shoulder at about 295°C.

containing 10, 15, or 20% SWNT-B, respectively). The peak T_d of composites containing 35 or 50% SWNT-B was lower than that of the neat PMMA.

Studies have been reported with both increases[27,42–52] and decreases[20,53–55] in the polymer T_d upon the addition of CNTs. The enhancement of the decomposition temperature in a nanocomposite with respect to the neat polymer has been interpreted as due to an interaction between the polymer and CNTs, in which the nanofiller acts as a restriction site, resulting in reduced segmental mobility of the polymer chains. The reduced mobility in turn assists in preventing scission of chains driven by thermal excitation.[56] No clear explanation is available for the decrease in the decomposition temperature. The enhancement of the peak T_d has also been explained in terms of a tortuous path effect.[57] It has been proposed that during the thermal degradation of clay/polymer nanocomposites, a protective surface barrier layer consisting of accumulated clay platelets with a small amount of carbonaceous char is formed.[58] Kashiwagi et al.[57] observed a network structure of accumulated CNTs after thermal degradation of the polymer. The network could increase the integrity of the protective layer and act as a barrier for the gas phase to diffuse into the bulk. Further studies are needed to fully understand the effects of nanomaterials on the polymer T_d.

The peak positions for the radical breathing mode (RBM), disorder-induced feature (D band), tangential mode (G band), and D-band overtone (G′ band) for all the composites are given in Table VIII. Both the RBM and D band positions remained almost the same for SWNT-B and SWNT-B/PMMA composites, whereas the G and G′ bands upshifted upon the addition of SWNT-B into the PMMA matrix. The shifts of the G (or G′) band were almost the same for all the composite films, regardless of the SWNT-B concentrations, in comparison with the SWNT-B powder. The full width at half-maximum (fwhm) of the G band (Table VIII) decreased with the SWNT-B loading increasing. Lefrant et al.[13] observed that G band widths decreased upon the addition of SWNTs into the PMMA matrix. The authors hypothesized

TABLE VIII
Raman Band Positions of Various Bands and fwhm Values of the G Band of SWNT-B and the SWNT-B/PMMA Composites

			G band		
SWNT-B (wt %)	RBM (cm^{-1})	D band (cm^{-1})	Position (cm^{-1})	fwhm (cm^{-1})	G′ band (cm^{-1})
0.5	266.7	1308.1	1593.1	29	2597.2
1	266.4	1308.7	1593.0	30	2597.1
5	266.4	1309.0	1592.8	29	2597.3
10	266.5	1309.5	1592.5	28	2597.9
15	267.2	1309.7	1592.2	27	2596.0
20	266.5	1308.4	1592.0	24	2596.3
35	267.0	1309.5	1592.5	25	2596.9
50	267.5	1308.6	1592.2	23	2596.0
100	266.5	1308.8	1589.0	24	2587.7

TABLE IX
Toluene Resistance of PMMA and the SWNT-B/PMMA Composites

	Weight loss (%)		
SWNT-B (wt %)	Based on the whole film weight (toluene exposure = 30 min)	Based on the PMMA weight (toluene exposure = 30 min)	Time in which the film disintegrated completely in toluene (h)
0	40.1	40.1	3
1	30.0	30.3	4
5	16.6	17.5	4
10	11.4	12.6	4
15	7.7	9.1	6
20	5.8	7.2	6
35	3.7	5.7	8
50	3.0	5.9	8

that the decrease in the G band width was caused by PMMA intercalation into SWNT bundles. At the same time, an upshift in RBM was observed when SWNTs were embedded into the PMMA matrix, although in our case RBM remained the same and the G band width increased after SWNTs were embedded into the PMMA matrix. Dresselhaus and Eklund[59] concluded that the greater the pressure on SWNTs, the wider the G band. In our case, it may be reasonable to consider that the pressure on SWNTs from the surrounding polymer matrix was higher at lower SWNT loadings, and so a broader G band was found. With the nanotube content increasing, the pressure on SWNTs caused by the surrounding polymer matrix decreased, and this resulted in the decreased width of the G band. Topological defects have also been reported to affect the G band width.[60] However, in our case, samples containing low nanotube concentrations were sonicated for less time, and yet these samples showed the broadest G band, whereas the G band width of the samples containing high nanotube concentrations that underwent longer sonication times was comparable to that of the G band width of the pristine nanotube sample that underwent no sonication. Therefore, we conclude that the G band width variations in our case were not related to the topological variations but perhaps were related to the pressure differences in different samples.

The solvent resistance of PMMA and SWNT-B/PMMA composite films was examined by the immersion of these films into toluene for 30 min at room temperature. The films were removed from toluene and dried in a vacuum oven at 80°C for 4 days to remove any traces of toluene. The weight changes in PMMA and SWNT-B/PMMA composites by their exposure to toluene for 30 min are given in Table IX. With increasing SWNT-B loadings, the weight loss based on the weight of the whole film decreased. The time that it took for the various samples to completely disintegrate is also listed in Table IX. For 35 and 50 wt % samples, it took about 8 h for the films to completely disintegrate. The decreased weight loss with increasing nanotube loading indicated increased solvent resistance of the composite in comparison with pure PMMA. From these observations, we conclude that the polymer closer to the CNTs takes longer to dissolve than the polymer farther away from them. Similar solvent resistance behavior has also been reported for PAN/CNT films[29] and fibers.[33,34]

SEM images of cross sections of MWNT/PMMA and VGCNF/PMMA composites are shown in Figure 11. Both MWNTs and VGCNFs dispersed uniformly in the PMMA matrix. In addition, Figure 11 shows that even after sonication, the MWNT and VGCNF structures were still intact. As mentioned earlier, work on PAN/MWNT and PAN/VGCNF

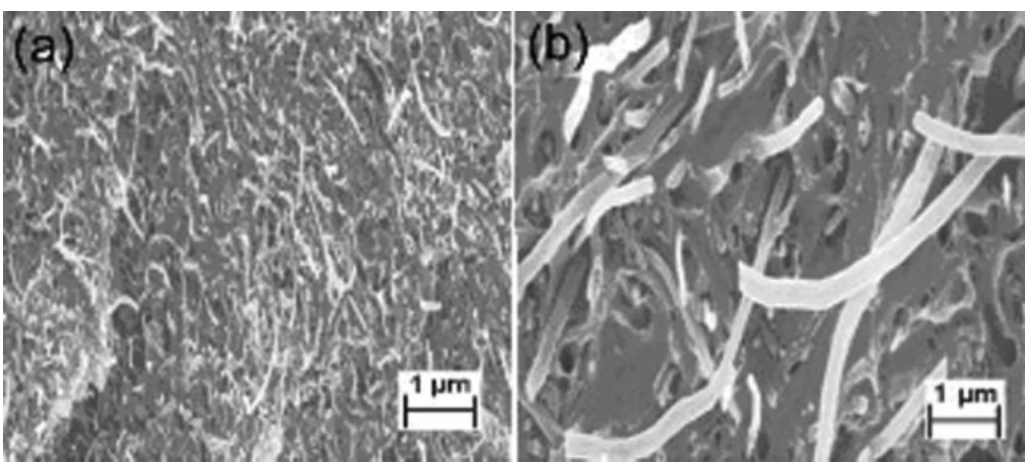

Figure 11 SEM images of sections of (a) MWNT/PMMA (15/85 weight ratio) and (b) VGCNF/PMMA (15/85 weight ratio).

TABLE X
Tensile Properties and Electrical Conductivity Values of the SWNT-A-, SWNT-B-, MWNT-, and VGCNF-Reinforced PMMA Composites with 15 wt % CNT

Sample	Tensile modulus (GPa)	Tensile strength (MPa)	Elongation at break (%)	Electrical conductivity (S/m)
PMMA film	1.8 ± 0.1	50 ± 8	3.5 ± 0.5	10×10^{-14} [62]
SWNT-A/PMMA (15/85)	4.1 ± 0.2	23 ± 12	0.6 ± 0.3	1430
SWNT-B/PMMA (15/85)	5.3 ± 0.2	71 ± 1	2.4 ± 0.2	854
MWNT/PMMA (15/85)	3.5 ± 0.6	54 ± 12	1.7 ± 0.4	15
VGCNF/PMMA (15/85)	3.2 ± 0.1	62 ± 21	1.9 ± 0.6	6

composite fibers also showed that nanotube structures remained intact after sonication.[34,36] The mechanical properties of various films are compared in Table X. At the same filler loading, SWNT-B had the highest reinforcement efficiency. MWNT and VGCNF composites exhibited moderate enhancements in tensile modulus and tensile strength. The difference in the reinforcing efficiency of SWNT-A and SWNT-B can be attributed to the presence of the metal catalyst in SWNT-A. The difference in the reinforcing efficiency of SWNT-B, MWNTs, and VGCNFs can be attributed to the differences in their diameters. The average diameter of SWNTs used in this study was in the range of 1–2 nm, whereas for the MWNTs, it was about 10–20 nm. The diameter of VGCNFs was in the range of 50–150 nm. A higher diameter nanotube results in a lower interfacial area between the nanofiller and the surrounding matrix, hence reducing the reinforcing efficiency. Electrical conductivity values for various films are also compared in Table X. Electrical conductivities of SWNT composite films were about 2 orders of magnitude higher than those of MWNT and VGCNF composite films. In a separate study, the surface areas of various CNT powders were measured with nitrogen gas adsorption and were analyzed with BET.[61] Experimentally determined surface area values were as follows: SWNT-A, 434 m^2/g; SWNT-B, 795 m^2/g; MWNTs, 161 m^2/g; and VGCNFs, 41 m^2/g. The mechanical property improvements and solvent resistance behavior of different types of CNTs followed the surface area trends.

Tan δ peak positions at different frequencies for PMMA, SWNT-A/PMMA, SWNT-B/PMMA, MWNT/PMMA, and VGCNF/PMMA containing 15 wt % CNT loadings are given in Table XI. At a given test frequency, the magnitude of the tan δ peak decreased and the peak temperature increased in the order of PMMA, VGCNF/PMMA, MWNT/PMMA, SWNT-A/PMMA, and SWNT-B/PMMA films. T_g's determined by the tan δ peak position at a frequency of 1 Hz were 121, 123, 123, 129, and 130°C for PMMA, VGCNF/PMMA, MWNT/PMMA, SWNT-A/PMMA, and SWNT-B/PMMA, respectively. The glass transition activation energies are listed in Table XI. The activation energies of the CNT/PMMA composites were comparable to that of the PMMA film.

As discussed previously, solvent resistance was examined through the dipping of the samples into toluene for 30 min at room temperature, and the weight loss is listed in Table XII. At the same CNT loading, SWNT-B/PMMA exhibited the highest solvent resistance, as evidence by a small loss of weight (7.7 and 10.8% for SWNT-B- and SWNT-A-containing composites, respectively) in comparison with a substantially higher weight loss for composites of MWNTs and VGCNFs (23.9 and 27.2%, respectively). The thermal degradation behavior of PMMA, SWNT-A/PMMA, SWNT-B/PMMA, MWNT/PMMA, and VGCNF/PMMA composites in air is

TABLE XI
Tan δ Peak Temperature (*P*) and Tan δ Peak Magnitude (*M*) Values for PMMA and the CNT/PMMA Films (15/85) at Different Frequencies and Calculated Activation Energies

	0.1 Hz		1 Hz		10 Hz		Activation energy
Sample	*P* (°C)	*M*	*P* (°C)	*M*	*P* (°C)	*M*	(kJ/mol)
PMMA	113	1.99	121	1.74	124	1.00	497
VGCNF/PMMA (15/85)	119	1.34	123	1.24	130	0.96	538
MWNT/PMMA (15/85)	120	0.82	123	0.74	131	0.72	519
SWNT-A/PMMA (15/85)	124	0.73	129	0.56	136	0.38	514
SWNT-B/PMMA (15/85)	123	0.43	130	0.35	137	0.32	444

TABLE XII
Toluene Resistance Values of Various Films

Sample	Weight loss (%)		Time in which the film disintegrated completely in toluene (h)
	Based on the whole film weight (toluene exposure = 30 min)	Based on the PMMA weight (toluene exposure = 30 min)	
PMMA	40.1	40.1	3
SWNT-B/PMMA (15/85)	7.7	9.1	6
SWNT-A/PMMA (15/85)	10.8	12.7	6
MWNT/PMMA (15/85)	23.9	28.1	3
VGCNF/PMMA (15/85)	27.2	32.0	3

TABLE XIII
T_d Values of Various Films Determined by TGA at a Heating Rate of 10°C/min

Sample	T_d (°C)		
	PMMA		
	In air	In nitrogen	Filler (CNT) in air
PMMA	337	388	—
SWNT-A/PMMA (15/85)	346	382	422
SWNT-B/PMMA (15/85)	357	376	570
MWNT/PMMA (15/85)	357	387	626
VGCNF/PMMA (15/85)	374	384	738

TABLE XIV
CTEs and Temperatures at a 1% Length Change for Various Films

	CTE (10^{-6}/°C)		Temperature at a 1% length change (°C)
	At 30°C	At 105°C	
PMMA	50	152	116
VGCNF/PMMA (15/85)	35	151	120
MWNT/PMMA (15/85)	30	93	126
SWNT-A/PMMA (15/85)	18	67	137
SWNT-B/PMMA (15/85)	9	47	144

compared in Table XIII and Figure 12. PMMA degraded at ~ 357°C in air in the SWNT-B/PMMA film, whereas it degraded at 374°C in the VGCNF/PMMA film. All four composites had T_d values comparable to that of the control PMMA film in nitrogen, and this indicates that the presence of CNTs does not affect PMMA degradation in nitrogen (Table XIII). The composite films also exhibited a smaller CTE than pure PMMA (Table XIV). The CTEs of various films followed this order: PMMA >

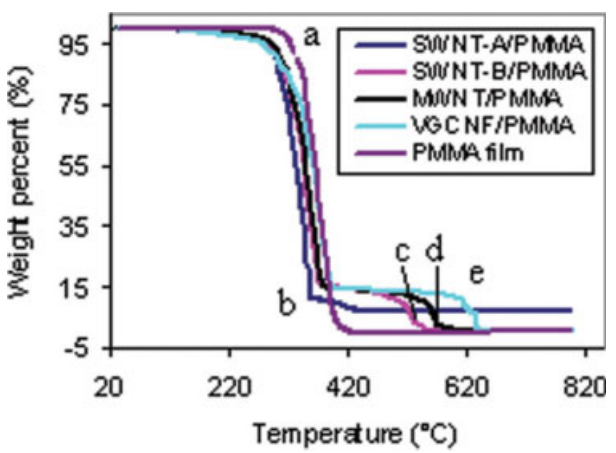

Figure 12 TGA in air at a heating rate of 10°C/min for (a) a PMMA film, (b) SWNT-A/PMMA (15/85), (c) SWNT-B/PMMA (15/85), (d) MWNT/PMMA (15/85), and (e) VGCNF/PMMA (15/85). [Color figure can be viewed in the online issue, which is available at www.interscience.wiley.com.]

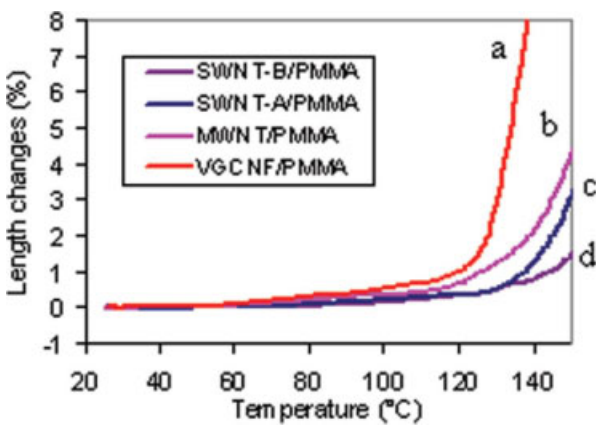

Figure 13 Thermal expansion of composite films as a function of temperature under 0.35-MPa stress at a heating rate of 5°C/min: (a) a VGCNF/PMMA film (15/85), (b) MWNT/PMMA (15/85), (c) SWNT-A/PMMA (15/85), and (d) SWNT-B/PMMA (15/85). [Color figure can be viewed in the online issue, which is available at www.interscience.wiley.com.]

VGCNF/PMMA > MWNT/PMMA > SWNT-A/PMMA > SWNT-B/PMMA (Fig. 13). For a 1% length change under 0.35-MPa stress, the temperature increased from 119°C for VGCNF/PMMA to 144°C for SWNT-B/PMMA. The results indicate that the composite containing SWNT-B had the highest dimensional stability.

CONCLUSIONS

On the basis of the dispersion study, nitromethane was employed as the solvent to process CNT/PMMA composites. SWNT-A (35.0 wt % catalyst)/PMMA, SWNT-B (2.4 wt % catalyst)/PMMA, MWNT/PMMA, and VGCNF/PMMA composite films with 15 wt % CNT loadings were processed. SWNT-B/PMMA composites with CNT loadings of 0.5, 1, 5, 10, 15, 20, 35, and 50 wt % were processed. For all these compositions, CNT dispersed uniformly into the PMMA matrix as evidenced by optical micrographs and SEM images. Relatively poor mechanical properties and dimensional stability of SWNT-A composites versus SWNT-B/PMMA composites were attributed to the presence of catalytic metal impurities. With the SWNT-B loading increasing, the dimensional stability ($\sim$ 96% reduction in CTE with a 50 wt % SWNT-B loading) and the solvent resistance were enhanced. As expected, the electrical conductivity of SWNT-B/PMMA increased with an increasing SWNT-B loading, with percolation at 0.5 vol % CNTs. The tensile modulus and the tensile strength did not increase linearly with increasing nanotube loading; they reached the maximum values with 35 wt % SWNT-B. The tensile properties and electrical conductivity values of the PMMA/CNT composites could be compared to the properties of PAN/CNT films and 100% CNT bucky paper.

Among the various CNT/PMMA composites studied in this article, the SWNT-B/PMMA composite film exhibited the highest enhancement of the tensile modulus, tensile strength, dimensional stability, and solvent resistance, and it was followed by composites of SWNT-A, MWNTs, and VGCNFs. An SWNT-A-reinforced PMMA composite had the highest electrical conductivity among these four CNT/PMMA composites. The higher electrical conductivity in the SWNT-A composites versus the SWNT-B composites was due to the additional conductivity network formed by the metal catalyst. T_d of PMMA in nitrogen did not vary significantly in the composites, indicating that CNTs by themselves did not affect the PMMA decomposition. Property improvements in various composites followed the trends observed for the CNT surface areas.

References

1. Bethune, D. S.; Kiang, C. H.; Devries, M. S.; Gorman, G.; Savoy, R.; Vazquez, J.; Beyers, R. Nature 1993, 363, 605.
2. Iijima, S.; Ichihashi, T. Nature 1993, 363, 603.
3. Sugai, T.; Yoshida, H.; Shimada, T.; Okazaki, T.; Shinohara, H. Nano Lett 2003, 3, 769.
4. Bandow, S.; Takizawa, M.; Hirahara, K.; Yudasaka, M.; Iijima, S. Chem Phys Lett 2001, 337, 48.
5. Iijima, S. Nature 1991, 354, 56.
6. Minus, M. L.; Kumar, S. JOM 2005, 57, 52.
7. Carneiro, O. S.; Covas, J. A.; Bernardo, C. A.; Caldeira, G.; Van Hattum, F. W. J.; Ting, J. M.; Alig, R. L.; Lake, M. L. Compos Sci Technol 1998, 58, 401.
8. Uchida, T.; Anderson, D. P.; Minus, M. L.; Kumar, S. J Mater Sci 2006, 41, 5851.
9. Bae, D. J.; Kim, K. S.; Park, Y. S.; Suh, E. K.; An, K. H.; Moon, J. M.; Lim, S. C.; Park, S. H.; Jeong, Y. H.; Lee, Y. H. Phys Rev B 2001, 64, 233401.
10. Bozovic, I.; Bozovic, N.; Damnjanovic, M. Phys Rev B 2000, 62, 6971.
11. Popov, V. N.; Van Doren, V. E.; Balkanski, M. Solid State Commun 2000, 114, 395.
12. Che, J. W.; Cagin, T.; Goddard, W. A. Nanotechnology 2000, 11, 65.
13. Stephan, C.; Nguyen, T. P.; de la Chapelle, M. L.; Lefrant, S.; Journet, C.; Bernier, P. Synth Met 2000, 108, 139.
14. Abraham, J. K.; Philip, B.; Witchurch, A.; Varadan, V. K.; Reddy, C. C. Smart Mater Struct 2004, 13, 1045.
15. Haggenmueller, R.; Gommans, H. H.; Rinzler, A. G.; Fischer, J. E.; Winey, K. I. Chem Phys Lett 2000, 330, 219.
16. Jia, Z. J.; Wang, Z. Y.; Xu, C. L.; Liang, J.; Wei, B. Q.; Wu, D. H.; Zhu, S. W. Mater Sci Eng A 1999, 271, 395.
17. Sung, J. H.; Kim, H. S.; Jin, H. J.; Choi, H. J.; Chin, I. J. Macromolecules 2004, 37, 9899.
18. Du, F. M.; Fischer, J. E.; Winey, K. I. J Polym Sci Part B: Polym Phys 2003, 41, 3333.
19. Sabba, Y.; Thomas, E. L. Macromolecules 2004, 37, 4815.
20. Ramanathan, T.; Liu, H.; Brinson, L. C. J Polym Sci Part B: Polym Phys 2005, 43, 2269.
21. Skakalova, V.; Dettlaff-Weglikowska, U.; Roth, S. Synth Met 2005, 152, 349.
22. Jin, Z. X.; Pramoda, K. P.; Goh, S. H.; Xu, G. Q. Mater Res Bull 2002, 37, 271.
23. Jin, Z.; Pramoda, K. P.; Xu, G.; Goh, S. H. Chem Phys Lett 2001, 337, 43.
24. Park, S. J.; Cho, M. S.; Lim, S. T.; Cho, H. J.; Jhon, M. S. Macromol Rapid Commun 2003, 24, 1070.
25. Hwang, G. L.; Shieh, Y. T.; Hwang, K. C. Adv Funct Mater 2004, 14, 487.
26. Gorga, R. E.; Cohen, R. E. J Polym Sci Part B: Polym Phys 2004, 42, 2690.
27. Zeng, J. J.; Saltysiak, B.; Johnson, W. S.; Schiraldi, D. A.; Kumar, S. Compos B 2004, 35, 173.
28. Liu, J.; Liu, T.; Kumar, S. Polymer 2005, 46, 3419.
29. Guo, H.; Sreekumar, T. V.; Liu, T.; Kumar, S. Polymer 2005, 46, 3001.
30. Zhang, X. F.; Liu, T.; Sreekumar, T. V.; Kumar, S.; Moore, V. C.; Hauge, R. H.; Smalley, R. E. Nano Lett 2003, 3, 1285.
31. Li, K.; Gao, X. L.; Roy, A. K. Mech Adv Mater Struct 2006, 13, 317.
32. Pryamitsyn, V.; Ganesan, V. Macromolecules 2006, 39, 844.
33. Sreekumar, T. V.; Liu, T.; Min, B. G.; Guo, H.; Kumar, S.; Hauge, R. H.; Smalley, R. E. Adv Mater 2004, 16, 58.
34. Chae, H. G.; Minus, M. L.; Kumar, S. Polymer 2006, 47, 3494.
35. Fornes, T. D.; Baur, J. W.; Sabba, Y.; Thomas, E. L. Polymer 2006, 47, 1704.
36. Chae, H. G.; Sreekumar, T. V.; Uchida, T.; Kumar, S. Polymer 2005, 46, 10925.

37. Shekhar, S.; Prasad, V.; Subramanyam, S. Mater Sci Eng B 2006, 133, 108.
38. Sreekumar, T. V.; Liu, T.; Kumar, S. Chem Mater 2003, 15, 175.
39. Zhang, X. F.; Sreekumar, T. V.; Liu, T.; Kumar, S. J Phys Chem B 2004, 108, 16435.
40. Liu, T.; Kumar, S. Nano Lett 2003, 3, 647.
41. Shaffer, M. S.; Windle, A. H. Adv Mater 1999, 11, 937.
42. Costache, M. C.; Wang, D. Y.; Heidecker, M. J.; Manias, E.; Wilkie, C. A. Polym Adv Technol 2006, 17, 272.
43. Xiong, J. W.; Zheng, Z.; Qin, X. M.; Li, M.; Li, H. Q.; Wang, X. L. Carbon 2006, 44, 2701.
44. Li, J.; Tong, L. F.; Fang, Z. P.; Gu, A. J.; Xu, Z. B. Polym Degrad Stab 2006, 91, 2046.
45. McNally, T.; Potschke, P.; Halley, P.; Murphy, M.; Martin, D.; Bell, S. E. J.; Brennan, G. P.; Bein, D.; Lemoine, P.; Quinn, J. P. Polymer 2005, 46, 8222.
46. Moon, S. I.; Jin, F.; Lee, C.; Tsutsumi, S.; Hyon, S. H. Macromol Symp 2005, 224, 287.
47. Wang, B.; Sun, G. P.; Sun, G.; He, X. F.; Liu, J. J. Acta Polym Sinica 2006, 3, 408.
48. Yang, J.; Lin, Y. H.; Wang, J. F.; Lai, M. F.; Li, J.; Liu, J. J.; Tong, X.; Cheng, H. M. J Appl Polym Sci 2005, 98, 1087.
49. Gao, J. B.; Itkis, M. E.; Yu, A. P.; Bekyarova, E.; Zhao, B.; Haddon, R. C. J Am Chem Soc 2005, 127, 3847.
50. Xia, H. S.; Song, M. Soft Matter 2005, 1, 386.
51. Choi, Y. K.; Sugimoto, K. I.; Song, S. M.; Endo, M. Mater Lett 2005, 59, 3514.
52. Xie, H. F.; Liu, B. H.; Yang, H.; Wang, Z. L.; Shen, J. Y.; Cheng, R. S. J Appl Polym Sci 2006, 100, 295.
53. Yang, S. Y.; Castilleja, J. R.; Barrera, E. V.; Lozano, K. Polym Degrad Stab 2004, 83, 383.
54. Xu, Y. S.; Ray, G.; Abdel-Magid, B. Compos A 2006, 37, 114.
55. Probst, O.; Moore, E. M.; Resasco, D. E.; Grady, B. P. Polymer 2004, 45, 4437.
56. Drozdov, A. D. Macromol Nanotechnol 2007, 43, 1681.
57. Kashiwagi, T.; Grulke, E.; Hilding, J.; Harris, R.; Awad, W.; Douglas, J. Macromol Rapid Commun 2002, 23, 761.
58. Gilman, J. W. Appl Clay Sci 1999, 15, 31.
59. Dresselhaus, M. S.; Eklund, P. C. Adv Phys 2000, 49, 705.
60. Wu, G.; Dong, J. M. Phys Rev B 2006, 73, 245.
61. Guo, H. Ph.D. Thesis, Georgia Institute of Technology, 2007.
62. Brandrup, J.; Immergut, E. H.; Grulke, E. A.; Bloch, D. R. Polymer Handbook; Wiley: New York, 1999.